Destabilization of the Thermohaline Circulation by Atmospheric Eddy Transports

MOTOTAKA NAKAMURA, PETER H. STONE, AND JOCHEM MAROTZKE

Center for Meteorology and Physical Oceanography, Massachusetts Institute of Technology, Cambridge, Massachusetts

(Manuscript received 29 September 1993, in final form 1 April 1994)

ABSTRACT

Simple process models have been developed to investigate the role of atmosphere–ocean feedbacks in the stability of the current mode of the thermohaline circulation in the North Atlantic. A positive feedback between the meridional atmospheric transport of moisture and the high-latitude sinking thermohaline circulation (EMT feedback) has been found to help destabilize the latter. The minimum perturbation required to shut off the high-latitude sinking is considerably smaller when this feedback is included. Also, the high-latitude sinking is shut off much faster with this feedback than without it, given a perturbation of the same magnitude. There is also a strong positive feedback between atmospheric heat transport and the thermohaline circulation, but this can be modeled accurately on the global scale by using a properly tuned Newtonian cooling law for the surface heat flux. Idealized flux adjustment experiments suggest that the sensitivity of the real climate is not represented well in coupled atmosphere–ocean general circulation models that require O(1) adjustments in the surface fluxes of heat and freshwater to simulate the current climate.

1. Introduction

Multiple equilibria are a robust phenomenon in models of the ocean's thermohaline circulation. These ocean models cover the entire range of complexity, from box models (e.g., Stommel 1961) to global-geometry general circulation models [GCMs, Maier-Reimer and Mikolajewicz 1988; see Marotzke (1990) and Weaver and Hughes (1992) for a systematic account]. A crucial feature in all these studies has been the employment of different kinds of surface boundary conditions for temperature and salinity, respectively. Sea surface temperature (SST) was either fixed or restored to a prescribed profile of "apparent atmospheric temperatures" (Haney 1971), with a typical restoring timescale of one month in the GCM studies (e.g., Marotzke and Willebrand 1991). These boundary conditions reflect a very strong coupling of surface heat flux to SST anomalies, tending to remove the latter within a few months [for scales O(1000 km), Davis 1976]. The surface salinity, however, has a negligible influence on evaporation and precipitation rates, and consequently surface salinity anomalies can persist on much longer timescales. Hence, it has been argued that the crudest, physically based surface boundary condition for salinity is prescribed evaporation minus precipitation (E–P). The combination of fixed (or nearly fixed) SST and prescribed surface freshwater fluxes has become known as "mixed boundary conditions" and gives rise to multiple equilibria. The stability of the equilibria, however, cannot be adequately investigated in models with mixed boundary conditions; while superior to the unphysical restoring law for surface salinity used in many modeling studies, they suppress a number of feedbacks in the coupled atmosphere–ocean system.

Willebrand (1993) lists three major feedbacks between the thermohaline circulation (assumed to have a strong sinking branch at high latitudes) and the high-latitude temperature and salinity (and hence density) fields. The first works as follows: a positive anomaly in the strength of the thermohaline circulation transports more salt poleward and tends to increase high-latitude salinities and hence surface densities, which strengthens deep water formation and thus reinforces the anomaly in the thermohaline overturning. This positive feedback between circulation and salinity is counteracted by additional northward heat transport, which acts to raise temperatures and thus lower densities; this in turn weakens convective activity and the thermohaline circulation. This second negative feedback is excluded if SST is fixed or is weak if SST is restored with a very short time constant, and may thus be underestimated in many ocean GCM studies (see, however, Zhang et al. 1993). A much longer restoring time scale would admit the feedback but would be inconsistent with the observed lifetimes of localized SST anomalies. It has been suggested that scale-dependent restoring coefficients would admit both the impact of ocean heat transport on (large-scale) SST and the rapid removal of smaller-scale SST anomalies (Bretherton 1982; Willebrand 1993; Rahmstorf and Willebrand 1994).

Corresponding author address: Dr. Mototaka Nakamura, Center for Meteorology and Physical Oceanography, MIT, Room 54-1717, Cambridge, MA 02139.

One of the most complicated feedbacks affecting the thermohaline circulation is the third feedback, which involves increases in evaporation when enhanced overturning leads to higher surface temperatures. Pure freshwater leaves the ocean, so the remaining water becomes saltier, if at least some of the additional water in the atmosphere is transported away. If all of it precipitates locally, there is no net effect, and fixed freshwater fluxes are appropriate as boundary conditions. It cannot even be excluded that, locally, E–P decreases, although the global integral of perturbation E–P must be zero. It has been argued (Warren 1983) that in the global thermohaline circulation the feedback involving evaporation acts in its amplifying variant, and outweighs the direct temperature effects on density. Mixed boundary conditions eliminate all the feedbacks but the one between thermohaline circulation and surface salinity, which gives rise to the existence of multiple equilibria and transitions between them. But an accurate stability analysis of the different steady states can only be performed if, at least, the other two feedbacks are included, and it is hard to predict which one of feedbacks two and three will prove more powerful.

An explicit model of atmospheric water vapor transport must be constructed to assess the effect of SST changes on the surface freshwater fluxes. Prior attempts with simplified models (Birchfield 1989; Stocker et al. 1992) have employed ad hoc assumptions about where anomalously evaporated water vapor precipitates and have investigated only the sensitivity of the solutions to different transport assumptions. Coupled atmosphere–ocean GCMs do calculate the atmospheric water vapor transport explicitly, but to date none of them has been able to simulate the current climate without introducing arbitrary adjustments in the surface freshwater flux (Manabe and Stouffer 1988; Manabe and Stouffer 1993; Washington and Meehl 1989; Cubasch et al. 1992). Thus the feedbacks in these GCMs are only present in distorted form.

We present here a simple process model that provides a dynamically based coupling of atmospheric moisture and heat fluxes to the SST distribution, based on a parameterization of atmospheric eddy fluxes that has been successfully applied in a zonally averaged atmospheric model (Stone and Yao 1990). Our model is thus a fully coupled atmosphere–ocean model, albeit in an extremely crude geometry. The model spans one hemisphere, with two boxes representing the atmosphere and three boxes representing one ocean basin. The model admits all the feedbacks discussed by Willebrand (1993), allowing the identification of the third one as a positive feedback, and furthermore includes a fourth feedback, which acts between the thermohaline circulation and atmospheric heat transport. With a suitable choice of parameters, the model has two stable equilibria, as in Stommel (1961). By turning on various feedbacks in turn, we investigate how the stability of the steady states to finite amplitude perturbations changes as a more complete atmosphere–ocean coupling is invoked.

The paper is organized as follows. Section 2 describes the models we use, and section 3 the experiments and their interpretation. Section 4 summarizes our results.

2. Models

a. Geometry and physics of model 1

The vertical cross section of the geometry of the most sophisticated model, which we call model 1, is illustrated in Fig. 1. The two top boxes, which represent the atmosphere, cover a hemisphere and the three lower boxes, which represent the ocean, span a 60° longitudinal sector between 10.44° and 75°N. The atmosphere is assumed to mix the heat perfectly in the longitudinal direction, so that the oceanic influence on the atmospheric energy budget is zonally homogeneous. All the boxes are separated at 35°N, where the observed zonal mean time-averaged net radiative forcing is close to zero and the northward transports of heat and moisture in the atmosphere are near their peaks (Stone 1978). Equatorward of 35°N, the zonal mean net radiative forcing is positive, while to the north it is negative. The box ocean model is based on that developed by Stommel (1961). The surface areas of the ocean boxes 1 and 2 are the same, so that the volume of box 1 is equal to the sum of those of boxes 2 and 3. The depth of box 1, D, is 4000 m and that of box 2, d, is 400 m for most of the experiments. The ocean boxes are conceptually connected by pipes through which water is transported. This configuration is chosen to crudely approximate the North Atlantic basin.

Temperature and salinity in each ocean box are denoted by T_n and S_n (n = 1, 2, 3), respectively. The temperatures of boxes 1 and 2 are interpreted to be the zonal mean surface temperatures at 55°N and 20°N,

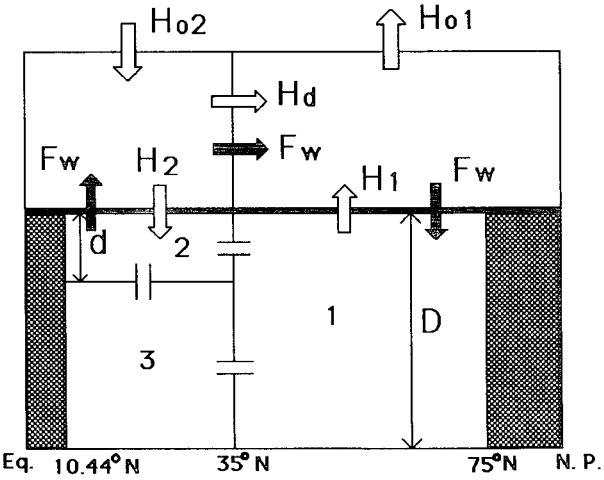

FIG. 1. Vertical cross section of model 1.

respectively. The volume flux due to the thermohaline circulation between two adjacent ocean boxes, q, is assumed to be proportional to the density difference between boxes 1 and 2 and given by

$$q = k[\alpha(T_2 - T_1) - \beta(S_2 - S_1)], \quad (1)$$

where k is a constant parameter with units of volume per unit time, and α and β are the thermal and haline expansion coefficients of seawater, respectively. Calculations with an ocean general circulation model support this simple parameterization for q (Hughes and Weaver 1994). We adopted the following values from a linearized equation of state: $\alpha = 1.5 \times 10^{-4}\,(\mathrm{K})^{-1}$ and $\beta = 8 \times 10^{-4}\,(\mathrm{ppt})^{-1}$. The volume flux is positive for high-latitude sinking, flowing from box 2 to 1, from box 1 to 3, and from box 3 to 2. Within each ocean box, instantaneous perfect mixing is assumed. Conceptually, all the physics of the thermohaline circulation (northward transport of warm and salty water, sinking of heavy water induced by intense cooling of the surface water by the atmosphere, which may involve freezing of water and ejection of salt, etc.) is contained in k. The density of water in boxes 1 and 2 is changed by advection of heat and salt and by exchange of heat and freshwater between the atmosphere and ocean. In box 3, it is affected only by advection of heat and salt. The time rates of change of the temperatures and salinities in the ocean boxes are given by the following six equations:

$$\frac{\partial T_1}{\partial t} = \frac{H_1}{C_w M_{w1}} + \frac{|q|(T_m - T_1)}{V_1},$$

$$m = 2 \text{ for } q > 0, \quad m = 3 \text{ for } q < 0, \quad (2)$$

$$\frac{\partial T_2}{\partial t} = \frac{H_2}{C_w M_{w2}} + \frac{|q|(T_m - T_2)}{V_2},$$

$$m = 3 \text{ for } q > 0, \quad m = 1 \text{ for } q < 0, \quad (3)$$

$$\frac{\partial T_3}{\partial t} = \frac{|q|(T_m - T_3)}{V_3},$$

$$m = 1 \text{ for } q > 0, \quad m = 2 \text{ for } q < 0, \quad (4)$$

$$\frac{\partial S_1}{\partial t} = -H_s \frac{V_1}{V_1} + \frac{|q|(S_m - S_1)}{V_1},$$

$$m = 2 \text{ for } q > 0, \quad m = 3 \text{ for } q < 0, \quad (5)$$

$$\frac{\partial S_2}{\partial t} = H_s \frac{V_1}{V_2} + \frac{|q|(S_m - S_2)}{V_2},$$

$$m = 3 \text{ for } q > 0, \quad m = 1 \text{ for } q < 0, \quad (6)$$

and

$$\frac{\partial S_3}{\partial t} = \frac{|q|(S_m - S_3)}{V_3},$$

$$m = 1 \text{ for } q > 0, \quad m = 2 \text{ for } q < 0, \quad (7)$$

where C_w is the specific heat of water; H_s is the virtual total salinity flux out of box 1; and V_n, M_{wn}, and H_n are the volume, mass of water, and the total surface heat flux (positive downward) for box n, respectively. The virtual salinity flux is related to the total net freshwater flux into the surface of ocean box 1, F_w, by $H_s = S_r(F_w/M_{w1})$, where we use 35 ppt for the reference salinity, S_r. The total salt mass in the ocean boxes is conserved.

Heat and moisture capacities of the atmosphere are assumed to be negligible. The surface fluxes of heat and freshwater are calculated by demanding energy and moisture conservation in the atmospheric boxes and diagnosing transports of heat and moisture at 35°N. The heat fluxes at the atmosphere–ocean boundary, H_1 and H_2, are calculated as the residue after the net radiative heating at the top of the atmospheric boxes, H_{o1} and H_{o2}, and the northward heat transport at 35°N, H_d, are calculated diagnostically (see Fig. 1). We assume that the baroclinic transient eddy transports constitute all of the meridional atmospheric transport, which is a good approximation at this latitude (Peixóto and Oort 1992). The latitudinal profile of the zonal mean surface temperature is approximated by the second Legendre Polynomial, $T_s(\phi) = T_{s0} + (T_{s2}/2) \times (3\sin^2\phi - 1)$, where ϕ is the latitude. Here T_{s0} and T_{s2} are obtained by fitting $T_s(\phi)$ to T_1 and T_2 at 55°N and 20°N, respectively. This temperature profile is used in the parameterized formulas for the net radiative forcing and the baroclinic eddy transports of heat and moisture.

The net radiative forcings, H_{o1} and H_{o2}, are parameterized by

$$H_{o1} = a_e^2 \int_0^{360°} \int_{35°}^{90°} [Q(1 - \hat{\alpha}_1) - F_t] \cos\phi d\phi d\lambda \quad (8)$$

and

$$H_{o2} = a_e^2 \int_0^{360°} \int_{0°}^{35°} [Q(1 - \hat{\alpha}_2) - F_t] \cos\phi d\phi d\lambda, \quad (9)$$

where λ is the longitude, a_e is the radius of the earth, Q is the time-averaged flux of solar radiation incident at the top of the atmosphere, F_t is the thermal longwave radiation flux, and $\hat{\alpha}_1$ and $\hat{\alpha}_2$ are the bulk mean albedos for the latitudinal belts 35°–90°N and 0°–35°N, respectively. For simplicity, we neglect ice-albedo feedback. Thus, the values of $\hat{\alpha}_1$ and $\hat{\alpha}_2$ are fixed at 0.40 and 0.25, respectively. These values yield the correct area- and Q-weighted global mean albedo, 0.3, and closely approximate the observed values. Here Q is approximated by

$$Q = \frac{Q_0}{4}\left[1 + \frac{Q_2}{2}(3\sin^2\phi - 1)\right], \quad (10)$$

where $Q_0 = 1365$ W m^{-2} and $Q_2 = -0.482$, as suggested by North (1975). The outgoing longwave radiation is parameterized by a linearized equation used by Wang and Stone (1980):

$$F_t = F_{t0} + \frac{dF_t}{dT_s} T_s. \tag{11}$$

The values of F_{t0} and dF_t/dT_s are taken from the results of a 1D radiative–convective equilibrium model with no ice albedo feedback and are 212 W m^{-2} and 1.7 W m^{-2} (°C)$^{-1}$, respectively. (Here, T_s has units of degrees Celsius.) With these approximations and parameterizations, (8) and (9) are readily evaluated.

The heat and moisture fluxes, H_d and F_w, are approximated by

$$H_d = a_e \cos 35° \int_0^{360°} \int_0^{\infty} [\rho_a(L_v \overline{v'\mu'} + C_p \overline{v'\theta'})] \times dz d\lambda, \tag{12}$$

and

$$F_w = \frac{A_t a_e \cos 35°}{6} \int_0^{360°} \int_0^{\infty} \rho_a \overline{v'\mu'} dz d\lambda, \tag{13}$$

where ρ_a is the atmospheric density, L_v is the latent heat of condensation, C_p is the specific heat of dry air at constant pressure, μ is the specific humidity or mixing ratio, and v and θ represent the meridional velocity and the potential temperature, respectively. Here $\rho_a \overline{v'\mu'}$ and $\overline{v'\theta'}$ are the meridional transient eddy fluxes of moisture and potential temperature, respectively. The overbar here denotes the time average and prime denotes deviation from the average. The atmospheric density is allowed to be a function of height only and is given by $\rho_a = \rho_{a0} e^{-(z/H)}$, where ρ_{a0} is the density of air at sea level and is 1.27 kg m^{-3}, and H is 8 km. Although $\rho_a C_p \overline{v'\theta'}$ includes the eddy flux of potential energy, we will refer to it as the eddy flux of sensible heat because the former is much smaller than the latter. Here, $\rho_a L_v \overline{v'\mu'}$ is the eddy flux of latent heat. Thus, the sum of $\rho_a L_v \overline{v'\mu'}$ and $\rho_a C_p \overline{v'\theta'}$ is the transient eddy heat flux.

Note that H_d is the heat transport for the entire longitudinal circle at 35°N since we assume perfect longitudinal mixing of heat in the atmosphere. However, F_w only represents that portion of the entire moisture transport at 35°N that comes out of the Southern Ocean and goes into the northern ocean. Here A_t is a constant parameter, which we call the Atlantic factor, that multiplies the baroclinic eddy transport of moisture in a 60° longitudinal sector at 35°N, so as to give a realistic haline forcing. This multiplicative constant is necessary to allow for the fact that a major portion of the water that enters the high-latitude North Atlantic is moisture that precipitates over land, and then enters the Atlantic as river runoff. Thus the effective moisture flux into the North Atlantic north of 35°N is considerably larger than the atmospheric transport across 35°N contained in a 60° longitudinal sector. Freshwater budgets compiled by Baumgartner and Reichel (1975) and Broecker et al. (1990) show that the net freshwater fluxes out of the Atlantic between 0° and 40°N and into the Atlantic north of 40°N are of similar magnitudes and correspond to a net loss of some 0.4 Sv (Sv $\equiv 10^6$ m^3 s^{-1}) between 0° and 40°N and net gain of about 0.3 Sv north of 40°N. Their studies suggest that A_t lies between 2 and 4. We assume that the rest of the moisture transported across 35°N in the atmosphere is returned to lower latitudes by rivers or underground flows; that is, we assume that the remaining moisture transport does not affect the Atlantic Ocean. Note that as long as $1 \leq A_t \leq 6$, the model is consistent in its energy and moisture budgets. The river runoff into the North Atlantic is positive if $A_t > 1$ and does not exceed the total net precipitation outside the 60° longitudinal Atlantic sector if $A_t \leq 6$.

For the two eddy transports, we adopt parameterizations from Stone and Yao (1990). They are based on Branscome's (1983) parameterization of $\overline{v'\theta'}$, which is in turn based on an approximate solution for the most unstable mode in the Charney (1947) model of baroclinic instability. The eddy amplitudes are determined by an equipartition assumption consistent with finite-amplitude eddy theories (Shepherd 1989, 1993). The parameterizations are

$$\overline{v'\theta'} = 0.6 \frac{g\kappa^2 N_w}{\tilde{\theta}_w f^2} \left(\frac{\partial \tilde{\theta}}{\partial y}\right)_w^2 e^{-(z/D_e)}(1 - e^{-(z/\delta z)}) \tag{14}$$

and

$$\overline{v'\mu'} = \tilde{h}\left(\frac{P}{P_0}\right)^{R/C_p} \frac{\partial \mu_s}{\partial T} \overline{v'\theta'}, \tag{15}$$

where $\tilde{}$) denotes the zonal mean, g is the gravitational acceleration, f is the Coriolis parameter, N is the Brunt–Väisälä frequency, h is the time-averaged relative humidity, μ_s is the saturation mixing ratio, R is the gas constant of dry air, P and P_0 are the atmospheric pressure and reference atmospheric pressure, respectively, and δz is the height of the planetary boundary layer. Here κ and D_e are height scales of the most unstable baroclinic wave and eddy meridional heat flux, respectively. Some details of these parameterizations are given in the appendix. With appropriate simplifying assumptions and approximations (see appendix), (12) and (13) can be analytically evaluated to obtain H_d and F_w as functions of T_1 and T_2. Then H_1, H_2, and H_s can be calculated from the atmospheric heat and moisture budgets.

We emphasize two important characteristics of these parameterizations. First, the transport of moisture and heat is proportional to roughly the 3.5 power of the meridional gradient of the zonal mean temperature in the lower part of the atmosphere, for a reasonable range

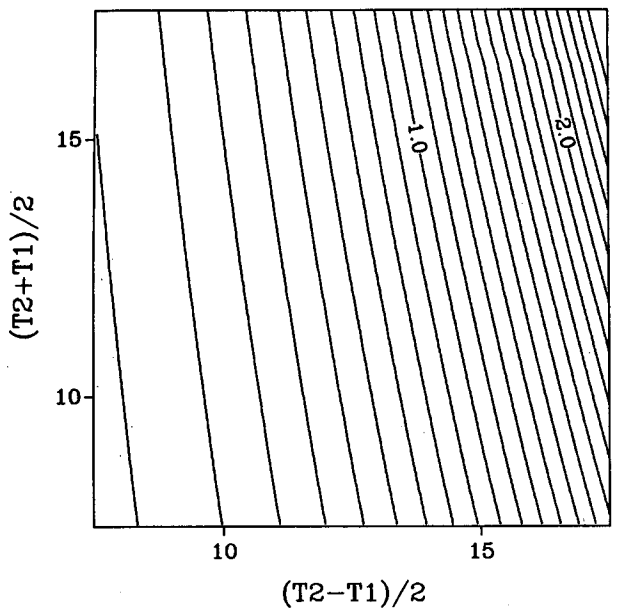

FIG. 2. For box 2, E–P (m yr^{-1}) with $A_t = 3$ as a function of $(T_1 + T_2)/2$ and $(T_2 - T_1)/2$ calculated by the baroclinic eddy transport parameterization. The contour interval is 0.1. The values of (T_1, T_2) for the left-bottom, left-upper, right-bottom, and right-upper corners, in degrees Celsius, are (0, 15), (10, 25), (−10, 25), and (0, 35), respectively.

of atmospheric conditions. Thus, an increase in the north–south temperature gradient enhances the northward freshwater transport and weakens the high-latitude oceanic sinking, which will in turn, further increase the north–south temperature difference because of the reduced oceanic heat transport. We will call this positive feedback the eddy moisture transport-thermohaline circulation feedback (EMT feedback). It plays a very important role in the destabilization of the thermohaline circulation discussed in section 3. Because of the strong (about 3.5 power) dependence of the moisture transport on the meridional temperature gradient, this positive feedback can amplify an initially small perturbation very rapidly. Held (1978) argued that the dependence should vary from the second to the fifth power of the meridional gradient of the zonal mean temperature, with the higher powers being favored when β effects are strong—that is, in low latitudes. An empirical study by Stone and Miller (1980) based on seasonal changes showed that the power varies from 1.6 ± 0.5 at 60°N to 3.4 ± 0.8 at 30°N, consistent with Held's result. We will test the sensitivity of our results to the exponent in this relationship later.

Second, the baroclinic eddy transport of moisture and latent heat has an exponential dependence on the atmospheric temperature, described by the Clausius–Clapeyron equation

$$\mu_s \approx 0.622 \frac{2.53 \times 10^{11}}{P} e^{-(5420/T)}. \qquad (16)$$

Thus the transports increase strongly with temperature. This effect has been noted frequently in GCM studies of global warming (e.g., Manabe et al. 1991). Figure 2 shows E–P (m yr^{-1}) for box 2 with $A_t = 3$ as a function of $(T_1 + T_2)/2$ and $(T_2 - T_1)/2$ calculated from the above parameterization. It illustrates these two characteristics of the parameterization of F_w. The effect of the meridional temperature gradient is manifested in the gradient of E–P parallel to the x axis, whereas that of the temperature at 35°N appears as the gradient in the y direction. As implied by the figure, in our experiments the former effect is considerably stronger than the latter.

Equations (2)–(7) are integrated in time, using a simple Euler time-stepping scheme, until equilibrium is reached. We used a time step of 30 days, which is small enough to prevent any numerical instability in our model.

b. *Tuning of model 1*

There are two parameters available to tune the model to mimic heat, salt, and water transports in the North Atlantic. The primary one is the proportionality constant, k, relating q to the density difference between boxes 1 and 2. There is also some room to vary the value of the Atlantic factor, A_t, as mentioned earlier, between 2 and 4. Because of the nonlinear relationship between k and A_t, the acceptable range of the two parameters is rather limited. This limitation on the range is mainly imposed by the need to simulate reasonably well both the haline forcing and the oceanic heat transport, while retaining the stability of the high-latitude sinking state. For instance, increasing k tends to make the volume flux larger, enhancing the northward oceanic heat transport and the stability of the high-latitude sinking cell. However, since the flushing of the boxes is strengthened due to the enhanced circulation, the temperature and salinity differences tend to be reduced. Therefore, a k increase must be accompanied by an increase in A_t within bounds imposed by observation. Also, keeping the northward heat transport by the meridional overturning cell, H_q, at around 1 PW, which is approximately the heat transport in the North Atlantic (Hall and Bryden 1982), puts an upper bound on k. It turned out that in order to realize at least 1.5 ppt salinity difference and satisfy the other requirements, k must be somewhere between 1.5×10^9 m^3 s^{-1} and 4.5×10^9 m^3 s^{-1}, given that A_t is somewhere between 2 and 4. After testing many choices for the parameter values, we picked one among many acceptable sets as the standard set, set 1. We also picked very stable and marginally stable sets, sets 2 and 3, respectively, for comparison.

These sets have the following parameter values:

set 1: $k = 2.77 \times 10^9$ m^3 s^{-1} and $A_t = 3$

set 2: $k = 2.77 \times 10^9$ m^3 s^{-1} and $A_t = 2$

set 3: $k = 2.65 \times 10^9$ m^3 s^{-1} and $A_t = 3$.

The high-latitude sinking equilibria of these sets are given in Table 1. Note that in our model, q is meant to represent that portion of the North Atlantic thermohaline circulation *that recirculates in the Northern Hemisphere.* Thus it should be about 10 Sv, not the 20 Sv total circulation found in global general circulation models that includes the cross-equatorial flow as well as the recirculation (e.g., Manabe et al. 1991; Marotzke and Willebrand 1991). Similarly, idealized 3D models of one hemisphere have a thermohaline circulation of only about 10 Sv (e.g., Marotzke 1990).

The chosen value of A_t for the reference set, 3, implies that half of the total meridional moisture transported across 35°N originates in the southern portion of the North Atlantic and flows into the northern portion. This value was chosen because it is the middle of the suggested range, 2–4. Here $F_w \approx 0.44$ Sv accompanied by $A_t = 3$ is equivalent to a net evaporation of 0.85 m yr^{-1} over box 2, a net precipitation of 0.28 m yr^{-1} over box 1, and river runoff of 0.57 m yr^{-1} into box 1, in reasonable agreement with Schmitt et al. (1989). The model's poleward heat transport in the ocean is also reasonably consistent with observations, which show a transport in the North Atlantic of 1.2 ± 0.3 PW at 24°N (Hall and Bryden 1982). However, this value represents the total heat transport, while the oceanic heat transport in our model represents only that portion due to the hemispherically closed thermohaline circulation. The atmospheric heat transport of 4.7 PW is somewhat larger than observed values, 3–4 PW at 35°N (Michaud and Derome 1991) because of the model's overestimated meridional gradient of surface temperature. At 35°N with parameter set 1, the model's gradient is 20% too large. This overestimate arises primarily because our model has only one ocean basin, and thus has no representation of the heat transport in the North Pacific, which is around 0.8 PW (Bryden et al. 1991). Most of this heat transport (and perhaps part of the transport in the North Atlantic) appears to be associated with wind-driven ocean circulations (Bryden et al. 1991) and therefore cannot be included in our model except through ad hoc, unphysical procedures. We preferred not to use such procedures, and therefore have accepted for our standard model a state in which the atmosphere accomplishes a larger proportion of the total heat transport than the actual atmosphere.

c. Models 2 and 3

To examine the role played by various feedback processes in model 1, we constructed two simpler models by replacing certain parameterizations by simpler ones. A version of intermediate complexity, which we call model 2, differs from model 1 in that the heat fluxes at the atmosphere–ocean boundary do not depend explicitly on the latitudinal temperature gradient and the radiative forcing. Instead, they are parameterized by the Newtonian cooling law, or restoring temperature condition (Haney 1971), given by

$$\frac{H_n}{C_w M_{wn}} = \frac{Te_n - T_n}{\tau_n}, \qquad (17)$$

where τ_n and Te_n are the thermal relaxation time and the surface equilibrium temperature, respectively, for Box n. Here Te_n is the equilibrium surface temperature, which would be attained if there were no oceanic heat transport. [See Bretherton (1982) and Marotzke (1993) for a detailed discussion of the concept of an atmospheric equilibrium surface temperature.] We calculated Te_n and τ_n from the two equilibria, one with a high-latitude sinking and the other with a low-latitude sinking obtained from model 1, for each of the three sets. We also calculated Te_n from the equilibria with zero oceanic heat transport. However, the differences between the values of Te_n obtained from these two methods are negligible (less than 0.01°C). Also, the differences between the values of τ_n obtained from the two methods are less than 2.5%. Thus, we used the values calculated from the first procedure in order to make the two equilibria in model 2 identical to their counterparts in model 1. These values of τ_n and Te_n for the three sets are listed in Table 1.

We note that τ_n is proportional to the depth of the ocean box. Since the deduced values of τ_2 are for a box 400-m deep, they are equivalent to a relaxation time of approximately one month for a layer 50-m deep. This is about half the value originally calculated by Haney (1971) and frequently used in ocean models with mixed boundary conditions (e.g., Marotzke and Willebrand 1991). As mentioned earlier, our model lacks another oceanic basin that carries about 0.8 PW northward. Our model compensates for this by producing a larger meridional temperature gradient and a larger heat flux in the atmosphere. Thus, the strength of the temperature relaxation in our model is likely to

TABLE 1. Characteristics of the high-latitude sinking solutions for the three sets of parameter choices mentioned in the text. Symbols are defined in the text; Sv ≡ 10^6m^{3}s^{-1} and 1 PW = 10^{15}W.

	Set 1	Set 2	Set 3
$T_1 = T_3$ (°C)	−1.85	−1.63	−1.97
T_2 (°C)	27.11	26.97	27.18
$S_1 = S_3$ (ppt)	33.897	33.949	33.875
S_2 (ppt)	35.956	34.968	36.379
q (Sv)	7.46	9.61	6.28
F_w (Sv)	0.439	0.280	0.449
$E - P$ (m yr^{-1})	0.849	0.542	0.868
$H_q = H_2 = -H_1$ (PW)	0.904	1.150	0.766
$H_{o1} = -H_{o2}$ (PW)	−5.644	−5.680	−5.624
H_d (PW)	4.740	4.530	4.858
Te_1 (°C)	−2.62	−2.62	−2.62
Te_2 (°C)	27.60	27.60	27.60
τ_1 (days)	2756	2779	2737
τ_2 (days)	177	178	175

be overestimated. In fact, when the missing northward heat transport in another ocean is included (in ad hoc fashion), the equivalent temperature restoring timescale for a layer 50-m deep is about two months.

Finally, the simplest version, model 3, uses mixed boundary conditions—that is, the Newtonian cooling parameterization of the surface heat fluxes used in model 2 and a constant freshwater flux. Model 3 differs from model 2 primarily in that it lacks the EMT feedback. The values of Te_n and τ_n used in model 2 and the high-latitude sinking equilibrium value of H_s from models 1 and 2 are used in model 3. Thus, model 3 has a high-latitude sinking equilibrium identical to those in models 1 and 2. However, since the two equilibria in models 1 and 2 have different values of H_s, the low-latitude sinking equilibrium of model 3 differs slightly from those of models 1 and 2.

3. Results and discussion

a. *Perturbation experiments*

We used the high-latitude sinking equilibria of sets 1, 2, and 3 as initial conditions and perturbed the system in various ways. We also tested the stability of the low-latitude sinking equilibria for comparison. We will mainly discuss negative S_1 perturbation experiments, which mimic a sudden increase in the freshwater flux in the high-latitude North Atlantic due to melting glaciers and pack ice. The results of these experiments are summarized in Table 2.

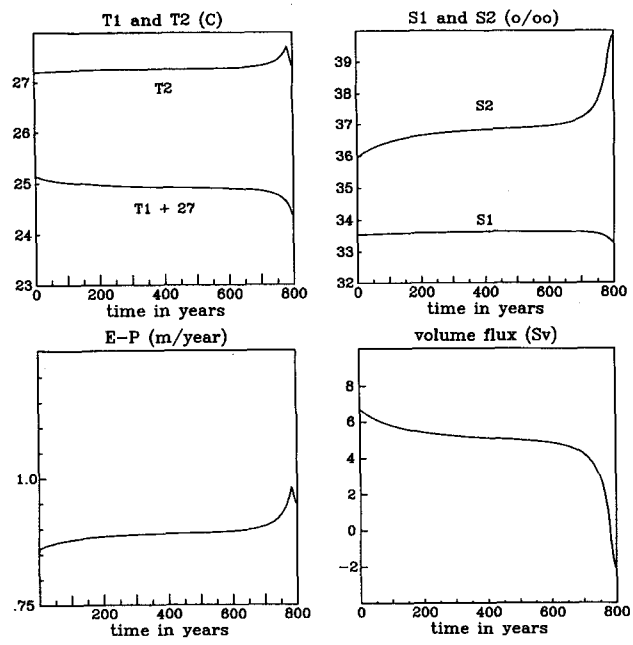

FIG. 3. The first 800 yrs of the time series of T_1, T_2, S_1, S_2, H_s, and q in the perturbation experiment with $S'_1 = -0.354$ ppt. The direction of the circulation never recovered for the rest of the run (up to 10 000 yr) after the reversal at around 770 years. For the curve of T_1, 27°C has been added. Model 1 and parameter set 1 are used.

TABLE 2. Circulation reversal time (yr) for various high-latitude salinity perturbations applied to the models with different parameter choices. Here S'_{1c} is the minimum perturbation required for the circulation to reverse.

Parameter set	Model	Initial perturbation in S_1 (ppt)	Circulation reversal time
1	1	$-0.354 \approx S'_{1c}$	770
		−0.359	450
		−0.53	160
	2	$-0.359 \approx S'_{1c}$	970
		−0.53	165
	3	$-0.53 \approx S'_{1c}$	370
2	1	$-1.87 \approx S'_{1c}$	360
		−1.89	220
		−2.14	105
	2	$-1.89 \approx S'_{1c}$	260
		−2.14	110
	3	$-2.14 \approx S'_{1c}$	310
3	1	$-0.056 \approx S'_{1c}$	1300
		−0.057	1100
		−0.15	260
	2	$-0.057 \approx S'_{1c}$	1990
		−0.15	270
	3	$-0.15 \approx S'_{1c}$	610

When we reduce S_1 sufficiently, by 0.354 ppt or more in model 1, with parameter set 1, the high-latitude sinking cell is shut off and a low-latitude sinking cell develops, shifting the system from one equilibrium to another as reported in other studies. Let a prime denote an initial deviation from equilibrium, and let a subscript "c" denote the critical value for switching the system from one equilibrium to another. Figure 3 shows the first 800-year evolution of T_1, T_2, S_1, S_2, q, and H_s, for a run with $S'_1 = -0.354$ ppt $\approx S'_{1c}$. The direction of the circulation reverses at around 770 yr and never recovers. (This integration was carried out for 10 000 yr.) Around year 700, the temperature gradient increases, leading to increased atmospheric moisture flux and hence increased salinity gradient in the ocean, thus causing the circulation to weaken dramatically. The time series clearly illustrate the EMT feedback, which works, for a negative S_1 perturbation, in the following manner:

(a) reduced high-latitude sinking → (b) reduced northward oceanic heat transport → (c) increased meridional temperature gradient (higher T_2 and lower T_1) → (d) increased northward transport of moisture by the atmosphere → (e) increased net evaporation in

low latitudes and net precipitation in high latitudes → (f) reduced S_1 and increased S_2 → (g) further reduced high-latitude sinking → (b).

Note that the feedback works in the opposite direction as well, although a positive S'_1 does not lead to a steady state with a stronger high-latitude sinking because there is only one high-latitude sinking equilibrium for a given set of k and A_t. With the aid of the EMT feedback, an initially moderate perturbation is amplified at first slowly, and then precipitously once the perturbation grows to a critical magnitude. In the new equilibrium, T_1 is decreased by about 0.50°C, while T_2 is increased by about 0.32°C. This new equilibrium, associated with a low-latitude sinking, is characterized by the following values of variables: $T_1 \approx -2.35$°C, $T_2 = T_3 \approx 27.43$°C, $S_1 \approx 30.439$ ppt, $S_2 = S_3 \approx 37.161$ ppt, $q \approx -2.52$ Sv, $H_q \approx 0.314$ PW, $F_w \approx 0.484$ Sv, $H_{o1} = -H_{o2} \approx -5.561$ PW, $H_d \approx 5.247$ PW, and $H_1 = -H_2 \approx -0.314$ PW.

This low-latitude sinking state is generally not represented well in box models. For example, comparisons between box models and idealized general circulation models suggest that inclusion of wind forcing inhibits development of low-latitude sinking equilibria, through Ekman and horizontal gyre transports (Marotzke 1990; Weaver et al. 1993; Winton and Sarachik 1993). The box models do not represent this aspect of more realistic models. Nevertheless, the differences between the two equilibria illustrate an interesting point: that is, small differences in the overall radiative balance of the climate system may be associated with large differences in the climate (Stone 1978). The two equilibria in our model obviously have very different climates; for example, the poleward oceanic heat transport in the low-latitude sinking state is only 35% of that in the high-latitude sinking state. In a realistic 3D model such a difference would be accompanied by large differences in regional temperatures—for example, in the vicinity of the North Atlantic. Nevertheless the total poleward heat transport ($H_d + H_q$) and the net radiative forcing (H_{o1} and H_{o2}) only differ by 1.5% in the two equilibria. The small differences in the global heat balance are due to the strong negative feedback between different components of the poleward heat transport; that is, the transport in the atmosphere increases to make up for most of the decrease in the ocean. This feedback is a fundamental characteristic of the climate system and is a common feature of climate models (Stone 1978).

We extended the S_1 perturbation experiments to models 2 and 3. Note that the high-latitude sinking equilibria in models 2 and 3 are identical to that in model 1, and thus the initial conditions for the experiments are the same as in model 1. Model 2 responds to initial salinity perturbations in much the same way as does model 1, but with slightly reduced sensitivity. For parameter set 1, when $S'_1 \leq -0.359$ ppt, model 2 settles into a low-latitude sinking equilibrium with a transient response very similar to that exhibited by model 1. With $S'_1 = -0.359$ ppt $\approx S'_{1c}$, it took approximately 970 yr for the circulation to be reversed. When this perturbation is applied to model 1, the circulation reverses at around 450 yr. Therefore, model 1 is only slightly more sensitive than model 2. Since the only part of model 1 that is not represented accurately in model 2 is the nonlinear dependence of the eddy heat transport, H_d, on the surface temperatures, this difference in the sensitivity between model 1 and model 2 is due to the different representations of the feedback in H_d (explicit in model 1, implicit through the definition of Te and τ in model 2).

There is, in fact, a positive feedback between H_d and the thermohaline circulation. As the high-latitude sinking becomes weaker, H_d increases, which tends to warm the high latitudes. Since warmer high latitudes tend to suppress the high-latitude sinking, the dependence of H_d on the meridional temperature gradient yields another positive feedback. Experiments with other parameter sets consistently show similar differences in the response of models 1 and 2. However, the differences are small, and thus, we suggest that the surface heat flux may be adequately parameterized on the global scale by the restoring surface temperature condition, if Te and τ are properly determined. However, this may not be the case for models, that are capable of responding to zonally asymmetric atmospheric forcing or have finer spatial structure than our model.

The differences in the sensitivity between models 1 and 3 are much larger than the differences between models 1 and 2, owing to the EMT feedback. The critical perturbation in model 3 with parameter set 1 is about −0.53 ppt; with this perturbation, models 1 and 2 develop a low-latitude sinking cell at around 160 and 165 years, respectively, while model 3 takes about 370 years. In model 3, H_s does not change in response to changes in the surface temperatures. Thus, the only way for model 3 to increase the salinity difference between boxes 1 and 2 is through the following feedback. A decrease in the high-latitude sinking circulation leads to reduced advection of salt from box 2 to 1, thereby making the left-hand side of Eqs. (5) and (6) more negative and positive, respectively, reinforcing the reduction of the high-latitude sinking. This is the first feedback referred to in the introduction and has been noted by other investigators (e.g., Walin 1985; Willebrand 1993). When the EMT feedback and this oceanic salt advection feedback reinforce each other, as in models 1 and 2, the sensitivity of the high-latitude sinking state is enhanced. We also note that when the temperatures are kept at equilibrium values in model 3 with parameter set 1—that is, the negative feedback due to the oceanic heat transport is removed by infinitely rapid temperature restoration—$S'_{1c} \approx -0.42$ ppt. This shows that the impact of oceanic heat transport on temperature has a stabilizing effect, which is however, weaker than the destabilizing effect of the

EMT feedback. This comparison does, however, depend on our choices of model parameters and needs to be investigated with a more realistic model. For example, when the atmospheric moisture transport is set proportional to the second power of the meridional gradient of the surface temperature, the two feedbacks have almost equal strength (see section 3b for details).

These sensitivity differences among the three models do not change when the perturbation is applied in different ways; model 1 is always the most sensitive among the three, model 2 is the next, and model 3 is the least sensitive, both in terms of the magnitude of perturbation required to switch the equilibrium and in terms of the time required for the circulation to reverse. For instance, when we perturb S_2, S'_{2c} is approximately 1.21 ppt, 1.22 ppt, and 1.52 ppt for models 1, 2, and 3, respectively.

b. *Parameter sensitivity tests*

We tested the sensitivity differences among the three models in cases with different values of k and A_t. Table 2 shows results for various choices of S'_1 for parameter sets 1, 2, and 3. Here τ_r is the time necessary for the initial high-latitude sinking to reverse. The qualitative differences among the three models are not affected by the values of these parameters. However, there are differences in how important the EMT feedback contribution is in the various parameter sets. These differences depend on the stability of the high-latitude sinking equilibria used for the initial conditions. When the haline forcing is weak, as in set 2, it takes a larger perturbation to force the system to move to the other equilibrium. The greater the stability of the system, the smaller is the impact of adding any feedback to it. Conversely, any feedback has a much stronger effect if the system is inherently less stable.

When the depth of box 2, d, is changed, the equilibria do not change. However, reducing d makes the system more sensitive to a perturbation, because the perturbed freshwater flux out of box 2, F_w, affects S_2 more, due to the reduced volume of the box, thereby enhancing the "braking effect" on q. This reinforces the perturbation and helps destabilize the system.

We also reconstructed our model with T_1 being set to the zonal mean temperature at 65°N rather than 55°N and repeated our experiments. We found no qualitative difference from the results described here.

Finally, we examined how the sensitivity of F_w and H_d to the meridional temperature gradient influences the sensitivity of model 1. The parameterizations used in model 1 (and also in model 2, for F_w) yield roughly a 3.5 power dependence of H_d and F_w on the meridional gradient of the zonal mean surface temperature at 35°N. As noted previously the correct power appears to vary with latitude (Stone and Miller 1980). Thus, we replaced the parameterizations given by (12)–(15) and (A1)–(A6) with simpler ones, which have a different dependence on the meridional temperature gradient. They are given by

$$\int_0^{360°}\int_0^{\infty} \rho_a \overline{v'\theta'} dz d\lambda = C_1\left(\frac{\partial T_s}{\partial y}\right)^n \qquad (18)$$

and

$$\int_0^{360°}\int_0^{\infty} \rho_a \overline{v'\mu'} dz d\lambda = \frac{C_2}{T_s^3} e^{-(5420/T_s)}\left(\frac{\partial T_s}{\partial y}\right)^n, \qquad (19)$$

where C_1 and C_2 are chosen to obtain a high-latitude sinking equilibria identical to that yielded by the full parameterizations in model 1 with parameter set 1. Then, S'_1 was applied to test the stability of the high-latitude sinking equilibrium.

In these sensitivity tests we picked $n = 2$ and $n = 0$. The former value is more appropriate for high latitudes (Stone and Miller 1980) and is the lower limit predicted by Held (1978). Taking $n = 0$ in effect removes the EMT feedback and the feedback between atmospheric and oceanic heat transports and gives us a test of their joint impact. We found that for $n = 2$, $S'_{1c} \approx -0.43$ ppt, and for $n = 0$, $S'_{1c} \approx -0.94$ ppt. These values may be compared with the result for model 1 with parameter set 1, for which $n \approx 3.5$ and $S'_{1c} \approx -0.354$ ppt. We see that the feedbacks between the atmospheric transports and the thermohaline circulation are still strongly destabilizing when $n = 2$. Thus our results are not critically dependent on an accurate representation of the dependence of the atmospheric fluxes on the meridional temperature gradient. Notice that the value $S'_{1c} \approx -0.43$ ppt with $n = 2$ is almost the same as the critical perturbation for model 3 without the THC heat transport feedback (see section 3a). This implies that the addition of the EMT feedback and the elimination of the THC heat transport feedback have destabilizing effects of comparable magnitudes for $n = 2$.

We may also compare the result for model 1 with $n = 0$, $S'_{1c} \approx -0.94$ ppt, with the result for model 3, $S'_{1c} \approx -0.53$ ppt. Both of these models exclude the EMT feedback, and their primary difference is that the former excludes the feedback between atmospheric and oceanic heat fluxes, while the latter includes it, albeit in a linearized form, through the Newtonian cooling law. Thus the difference between these two values of $S'1c$ shows that this feedback by itself is also strongly destabilizing, because it weakens the negative feedback between the thermohaline circulation and its heat transport. In effect, when H_q changes, H_d changes in the opposite way, reducing the negative feedback between H_q and q. However, as we noted earlier, this effect is modeled quite well by the Newtonian cooling law in our simple model, as long as τ and Te are chosen properly.

c. *Flux adjustment experiments*

Drifting to equilibria that do not resemble the current climate is a common problem among sophisticated

TABLE 3. Sensitivity of the standard model with flux adjustments, as measured by the minimum destabilizing perturbations, S'_{1c}. The two columns on the left show the assumed percentage errors in H_d and F_w. The next two columns show the required (time independent) flux adjustments for H_d and F_w. They are positive when they are added to (extracted from) box 2 (box 1). Units are PW for H_d, Sv for F_w, and ppt for S'_{1c}.

$H_{d(\text{err})}$	$F_{w(\text{err})}$	$H_{(\text{adj})}$	$F_{w(\text{adj})}$	S'_{1c}
0	0	0	0	−0.354
+100%	0	4.74	0	−0.381
−50%	0	−2.37	0	−0.316
0	+100%	0	0.44	−0.221
0	−50%	0	−0.22	−0.433
+100%	+100%	4.74	0.44	−0.299
−50%	−50%	−2.37	−0.22	−0.444

coupled GCMs (e.g., Manabe and Stouffer 1988; Washington and Meehl 1989). The cause of this problem has not been identified. Because of it, the fluxes of heat and freshwater at the oceanic surface in coupled GCMs must be adjusted by large amounts to obtain the current climate (Manabe and Stouffer 1988; Cubasch et al. 1992). The implied errors in the models' calculations of surface fluxes may cause the atmosphere–ocean interactions to be distorted.

We used model 1 to investigate how climate sensitivity may be altered in models that require artificial adjustments in the surface fluxes. Our approach is as follows. We adopt the high-latitude sinking equilibrium of set 1 as the "real world." Then, we alter H_d and/or F_w by multiplying them by constants to create "model worlds" with discrepancies from the "real world." The "model worlds" are forced to be identical to the "real world" by adjusting the surface fluxes of heat and/or freshwater. As in coupled GCMs, the adjusted portion of the fluxes is fixed in time. Finally, S'_1 is applied to the "model world" equilibria to see how the sensitivity compares with that of the "real world."

Many combinations of "errors" in H_d and F_w were tested. The resulting flux adjustments and S'_{1c} for six combinations are shown in Table 3. Clearly, underestimation of H_d and overestimation of F_w tend to reduce the stability of the equilibria, and vice versa, with one exception. When both H_d and F_w are underestimated by 50%, the effect of underestimated H_d is *stabilizing,* instead of destabilizing (cf. the case of underestimated F_w only). This effect may be due to the nonlinearity of the positive feedback between H_d and the thermohaline circulation, mentioned in section 3. Underestimation of H_d, in general, reduces the stability of the THC because it reduces the strong atmospheric negative feedback, which tends to suppress changes in the meridional temperature gradient, thereby enhancing the EMT feedback. Overestimation of F_w clearly enhances the EMT feedback, which tends to destabilize the THC. It appears to be a rule that the "model world" is more/less stable when the freshwater flux is underestimated/overestimated. Furthermore, errors in F_w have a larger effect than errors in H_d. One should note that errors in q also result in errors in the surface fluxes of heat and freshwater, which must be flux adjusted to obtain the correct state. As mentioned before, overestimated/underestimated q tends to stabilize/destabilize the system. This holds true in flux adjustment experiments as well (not shown).

Not only the sensitivity but also the transient response of a model is affected by these error factors considerably. Figure 4 shows an example of such differences in the transient response to a perturbation, which is, in this case, $S'_1 = -0.354$ ppt. Model 1A here is flux adjusted to compensate for a 100% overestimate in F_w. A qualitatively similar error occurs in the GFDL coupled GCM (Manabe et al. 1991). In particular, the GFDL GCM's unadjusted simulation of the moisture flux across 35°N is about twice the flux in the adjusted simulation, and the flux of moisture into the oceans near 60°N where North Atlantic Deep Water forms in the GCM is more than twice as much in the unadjusted case as in the adjusted case. The figure indicates that coupled atmosphere–ocean GCMs with such an error pattern may underestimate the stability of the THC considerably, by overestimating the strength of the EMT feedback.

4. Concluding remarks

By comparing the results produced by thermohaline circulation process models with different levels of so-

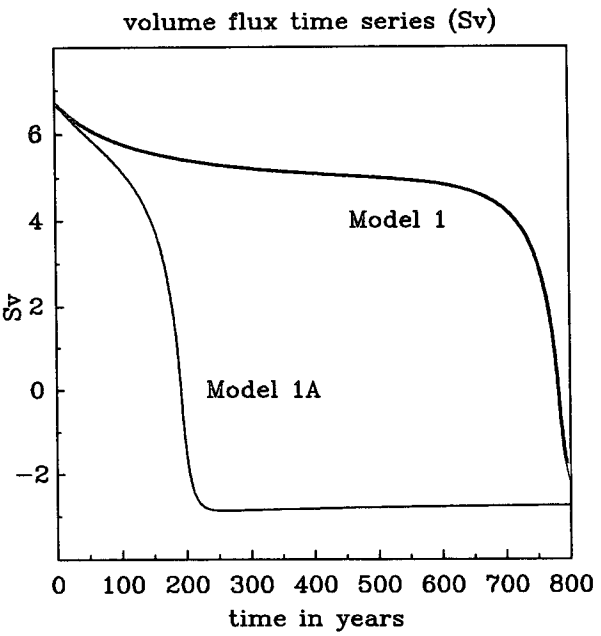

FIG. 4. The first 800 years of the time series of q in the perturbation experiment with $S'_1 = -0.354$ ppt, without (model 1) and with (model 1A) flux adjustment. The flux adjustment compensates for a 100% overestimate of F_w. In both experiments, which were integrated for 10 000 yr, the circulation never reverses back once it switches to the low-latitude sinking state.

phistication, we have found that using a coupled atmosphere–ocean model for calculating the surface freshwater flux is crucial to modeling the sensitivity of the thermohaline circulation accurately. The sensitivity to perturbations is greater when the surface freshwater flux is calculated from an interactive poleward transport of moisture in the atmosphere. This transport increases as the meridional gradient of the surface temperature increases, constituting a positive feedback between the atmospheric moisture transport and the thermohaline circulation. This feedback, which we call "the eddy moisture transport-thermohaline circulation (EMT) feedback," works in the following way:

(a) reduced high-latitude sinking → (b) reduced northward oceanic heat transport → (c) increased meridional temperature gradient (higher T_2 and lower T_1) → (d) increased northward transport of moisture by the atmosphere → (e) increased net evaporation in low latitudes and net precipitation in high latitudes → (f) reduced S_1 and increased S_2 → (g) further reduced high-latitude sinking → (b).

The EMT feedback is positive and reinforces the positive salt advection feedback in the ocean, resulting in a higher sensitivity of the thermohaline circulation in the coupled atmosphere–ocean system. There is also a strong positive feedback between the thermohaline circulation and the meridional transport of heat by atmospheric eddies in our coupled model. However, our results indicate that the conventional representation of the surface heat flux used in ocean models, that is, the Newtonian relaxation, can simulate this feedback reasonably well on the global scale, if the apparent equilibrium temperature and restoring times are properly determined.

There has emerged a consensus that oceanic GCMs employing mixed boundary conditions (in particular, use of Newtonian cooling with a short restoring timescale) overestimate the thermohaline circulation's sensitivity to the mean freshwater fluxes and time-dependent perturbations [e.g., the summary given by Stocker and Broecker (1992)]. Experiments with weak (Zhang et al. 1993) or scale-dependent (Rahmstorf and Willebrand 1994) restoring have indeed shown much increased stability of the thermohaline circulation. We have found that our coupled model, with the standard set of parameters, exhibits greater sensitivity to salinity perturbations than does the model with fixed temperature and fixed freshwater flux, meaning that the EMT feedback is stronger than the negative feedback between oceanic heat transport and the thermohaline circulation. A more realistic model must be used to test the robustness of this result; in particular, it would be important to know what the effective atmospheric equilibrium temperatures and restoring coefficients would be in a coupled GCM. To our knowledge, such a test has not been performed in a GCM, nor has it been tested how much a coupled GCM would be stabilized if the dependence of atmospheric moisture transport on the temperature structure were eliminated. However, the absence of the EMT feedback in the models of Zhang et al. (1993) and Rahmstorf and Willebrand (1994) means that these models probably overestimate the stability of the thermohaline circulation.

Finally, errors in the atmospheric and/or oceanic parts of coupled models, which require adjustments in the surface fluxes in order to obtain a realistic climate, may alter the sensitivity and transient behavior of a model substantially. Thus, results from coupled models that require adjustments in the surface fluxes must be interpreted with caution.

Acknowledgments. Fifty percent ($40,000) of this research was supported by the U.S. Department of Energy's (DOE) National Institute for Global Environmental Change (NIGEC) through the NIGEC Northeast Regional Center at Harvard University (DOE Cooperative Agreement DE-FC03-90ER61010). The remaining part was supported by the National Science Foundation (NSF) and the Tokyo Electric Power Company (TEPCO). Financial support does not constitute an endorsement by DOE, NSF, or TEPCO of the views expressed in this article. We also wish to thank S. Manabe and two anonymous referees for comments that were helpful in improving the clarity of the manuscript.

APPENDIX

Details of the Eddy Transport Parameterizations

Some more details of the parameterizations given by Eqs. (12)–(15) are described in the following. Notations and symbols are defined by

$$x_w = \frac{1}{D_e}\int_0^\infty xe^{-(z/D_e)}dz, \tag{A1}$$

$$\kappa = \frac{H_w}{1+\gamma}, \tag{A2}$$

$$\gamma = \frac{\beta N_w^2 H_w}{f^2\left(\dfrac{\partial \tilde{u}}{\partial z}\right)_w}, \tag{A3}$$

and

$$D_e = \frac{H_w}{(4K^2+1)^{1/2}-1} \approx \frac{H_w}{0.48+1.48\gamma}, \tag{A4}$$

where $\beta = df/dy$, u is the zonal velocity, and K is the total wavenumber of the most unstable mode, multiplied by NH/f. These parameterizations have been tested by Stone and Yao (1990) and found to work well in their zonally averaged 2D statistical-dynamical climate model. For more details of the derivation of these formulas we refer the reader to Stone and Yao (1990) and references therein.

In evaluating Eqs. (12) and (13) analytically at 35°N, simplifying assumptions are made. The following values are fixed: $H_w = 8$ km, $f = 8.4 \times 10^{-5}\ s^{-1}$, $\beta = 1.9 \times 10^{-11}\ s^{-1}\ m^{-1}$, $N_w^2 = 1.7 \times 10^{-4}\ s^{-2}$, $\tilde{h} = 0.8$, $\delta z = 450$ m, and $\tilde{\theta}_w = 300$°K. Since $R/C_p \approx 0.256$ and $0.5 \leq P/P_0 \leq 1.0$ in the region where most of the transport takes place, we simply set $(P/P_0)^{R/C_p} = 1.0$. We also assume that the thermal wind relation holds; namely,

$$\left(\frac{\partial \tilde{u}}{\partial z}\right)_w \approx \frac{\partial \tilde{u}}{\partial z} \approx -\frac{g}{f T_s}\frac{\partial T_s}{\partial y}. \qquad \text{(A5)}$$

To model vertical variation in $\partial \mu_s / \partial T$, which is not negligible, the vertical temperature structure is approximated by $T(35°\text{N}) = T_s(35°\text{N}) - \Gamma z$, where $\Gamma = 5$ K/km. This distribution is inserted into the Clausius–Clapeyron equation and the exponent is linearized about T_s. We obtain

$$\frac{\partial \mu_s}{\partial T} \approx \frac{2.97 \times 10^{12}}{\rho_a T_s^3} e^{-(5420/T_s)(1+(\Gamma z/T_s))} \qquad \text{(A6)}$$

(Here, T_s has units of kelvins.) This simplification is justifiable since a typical value of D_e is 3–4 km and changes in the variables that are assumed constant are small and would have negligible effects on H_d and F_w, compared to those allowed to vary. Consistent with the above approximations, we replace $(\partial \tilde{\theta}/\partial y)_w$ by $\partial T_s/\partial y$. With these approximations and assumptions, Eqs. (12) and (13) can be analytically evaluated to obtain H_d and F_w.

REFERENCES

Baumgartner, A., and E. Reichel, 1975: *Die Weltwasserbilanz.* Oldenbourg, 179 pp.

Birchfield, G. E., 1989: A coupled ocean–atmosphere climate model: Temperature vs. salinity effects on the thermohaline circulation. *Climate Dyn.*, **4**, 57–71.

Bretherton, F. P., 1982: Ocean climate modeling. *Progress in Oceanography,* Vol. 11, Pergamon, 93–129.

Branscome, L. E., 1983: A parameterization of transient eddy heat flux on a beta-plane. *J. Atmos. Sci.*, **40**, 2508–2521.

Broecker, W., T.-H. Peng, J. Jouzel, and G. Russell, 1990: The magnitude of global fresh-water transports of importance to ocean circulation. *Climate Dyn.*, **4**, 73–79.

Bryden, H. L., D. H. Roemmich, and J. A. Church, 1991: Ocean heat transport across 24°N in the Pacific. *Deep-Sea Res.*, **38**, 297–324.

Charney, J. G., 1947: The dynamics of long waves in a baroclinic westerly current. *J. Meteor.*, **4**, 135–162.

Cubasch, U., K. Hasselmann, H. Höck, E. Maier-Reimer, U. Mikolajewicz, B. Santer, and R. Sausen, 1992: Time-dependent greenhouse warming computations with a coupled ocean-atmosphere model. *Climate Dyn.*, **8**, 55–69.

Davis, R. E., 1976: Predictability of sea surface temperature and sea level pressure anomalies over the North Pacific Ocean. *J. Phys. Oceanogr.*, **6**, 249–266.

Hall, M. M., and H. L. Bryden, 1982: Direct estimates and mechanisms of ocean heat transport. *Deep-Sea Res.*, **29**, 339–359.

Haney, R. L., 1971: Surface thermal boundary condition for ocean circulation models. *J. Phys. Oceanogr.*, **1**, 241–248.

Held, I. M., 1978: The vertical scale of an unstable baroclinic wave and its importance for eddy heat flux parameterizations. *J. Atmos. Sci.*, **35**, 572–576.

Hughes, T. M. C., and A. J. Weaver, 1994: Multiple equilibria of an asymmetric two-basin ocean model. *J. Phys. Oceanogr.*, **24**, 619–637.

Maier-Reimer, E., and U. Mikolajewicz, 1988: Experiments with an OGCM on the cause of the Younger Dryas. *Oceanography 1989,* Ayala-Castanares, W. Wooster, and A. Yanez-Arancibia, Eds., UNAM Press, 87–100.

Manabe, S., and R. J. Stouffer, 1988: Two stable equilibria of a coupled ocean–atmosphere model. *J. Climate,* **1**, 841–866.

——, and ——, 1993: Century-scale effects of increased atmospheric CO_2 on the ocean–atmosphere system. *Nature,* **364**, 215–218.

——, ——, M. J. Spelman, and K. Bryan, 1991: Transient responses of a coupled ocean–atmosphere model to gradual changes of atmospheric CO_2. Part 1: Annual mean response. *J. Climate,* **4**, 785–818.

Marotzke, J., 1990: Instabilities and multiple equilibria of the thermohaline circulation. Ph.D. thesis, Report of the Institut für Meereskunde Kiel No. 194, 126 pp.

——, 1994: Ocean models in climate problem. *Ocean Dynamics in Climate Processes.* P. Malanotte-Rizzoli and A. R. Robinson, Eds., NATO ASI Series, Kluwer, 79–109.

——, and J. Willebrand, 1991: Multiple equilibria of the global thermohaline circulation. *J. Phys. Oceanogr.*, **21**, 1372–1385.

Michaud, R., and J. Derome, 1991: On the mean meridional transport of energy in the atmosphere and oceans as derived from six years of ECMWF analyses. *Tellus,* **43a**, 1–14.

North, G. K., 1975: Theory of energy-balance climate models. *J Atmos. Sci.*, **32**, 2033–2043.

Peixóto, J. P., and A. H. Oort, 1992: *Physics of Climate.* American Institute of Physics, 520 pp.

Rahmstorf, S., and J. Willebrand, 1994: The role of temperature feedback in stabilizing the thermohaline circulation. *J. Phys. Oceanogr.*, in press.

Schmitt, R., P. Bogden, and C. E. Dorman, 1989: Evaporation minus precipitation and density fluxes for the North Atlantic. *J. Phys. Oceanogr.*, **19**, 1208–1221.

Shepherd, T. G., 1989: Nonlinear saturation of baroclinic instability. Part II: Continuously stratified fluid. *J. Atmos. Sci.*, **46**, 888–907.

——, 1993: Nonlinear saturation of baroclinic instability. Part III: Bounds on the energy. *J. Atmos. Sci.*, **50**, 2697–2709.

Stocker, T. F., and W. S. Broecker, 1992: NADW formation as a branch of the hydrological cycle. *Eos, Trans. Amer. Geophys. Soc.*, **73**(18), 202–203.

——, D. G. Wright, and L. A. Mysak, 1992: A zonally averaged coupled ocean–atmosphere model for paleoclimatic studies. *J. Climate,* **5**, 773–797.

Stommel, H., 1961: Thermohaline convection with two stable regimes of flow. *Tellus,* **13**, 224–230.

Stone, P. H., 1978: Baroclinic adjustment. *J. Atmos. Sci.*, **35**, 561–571.

——, and D. A. Miller, 1980: Empirical relations between seasonal changes in meridional temperature gradients and meridional fluxes of heat. *J. Atmos. Sci.*, **37**, 1708–1721.

——, and M.-S. Yao, 1990: Development of a two-dimensional zonally averaged statistical-dynamical model. Part III: The parameterization of the eddy fluxes of heat and moisture. *J. Climate,* **3**, 726–740.

Walin, G., 1985: The thermohaline circulation and the control of ice ages. *Palaeogeogr., Palaeoclimatol., Palaeoecol.*, **50**, 323–332.

Wang, W.-C., and P. H. Stone, 1980: Effect of ice-albedo feedback on global sensitivity in a one-dimensional radiative-convective climate model. *J. Atmos. Sci.*, **37**, 545–552.

Warren, B. A., 1983: Why is no deep water formed in the North Pacific? *J. Mar. Res.*, **41**, 327–347.

Washington, W. M., and G. A. Meehl, 1989: Climate sensitivity due to increased CO_2: Experiments with a coupled atmosphere and ocean general circulation model. *Climate Dyn.*, **4,** 1–38.

Weaver, A. J., and T. M. C. Hughes, 1992: Stability and variability of the thermohaline circulation and its link to climate. *Trends Phys. Oceanogr.*, **1,** 15–70.

——, J. Marotzke, P. F. Cummins, and E. S. Sarachik, 1993: Stability and variability of the thermohaline circulation. *J. Phys. Oceanogr.*, **23,** 39–60.

Willebrand, J., 1993: Forcing the ocean with heat and freshwater fluxes. *Energy and Water Cycles in the Climate System,* E. Raschke, Ed., Springer-Verlag, 215–233.

Winton, M., and E. S. Sarachik, 1993: Thermohaline oscillations induced by strong steady salinity forcing of ocean general circulation. *J. Phys. Oceanogr.*, **23,** 1389–1410.

Zhang, S., R. J. Greatbatch, and C. A. Lin, 1993: A re-examination of the polar halocline catastrophe and implications for coupled ocean–atmosphere modelling. *J. Phys. Oceanogr.*, **23,** 287–299.